MODELING NONEQUILIBRIUM CONTAMINANT TRANSPORT PROCESSES IN SOILS AND GROUNDWATER

Martinus Th. van Genuchten[1,*], Elizabeth M. Pontedeiro[2], and Renato M. Cotta[1]
[1]Department of Mechanical Engineering, COPPE/LTTC, Federal University of Rio de Janeiro, UFRJ, Rio de Janeiro, RJ, 21945-970, Brazil
[2]Radioactive Waste Division, DIREJ, Brazilian Nuclear Energy Commission, CNEN, Rua da Passagem 123, Botafogo, Rio de Janeiro, RJ, 20290-030, Brazil
(*Corresponding author: rvangenuchten@yahoo.com)

ABSTRACT. Accurate simulation of contaminant transport processes in the subsurface remains a major challenge in many science and engineering applications. In this paper we review a broad range of dual-porosity and dual-permeability formulations for modeling nonequilibrium or preferential fluid flow and contaminant transport in macroporous soils or fractured rock. We focus especially on transport processes in the variably-saturated vadose zone between the soil surface and the groundwater table. One effective modeling approach for flow is to use composite functions for the unsaturated hydraulic conductivity to account for the separate effects of macropores and micropores, and to combine this approach with a mobile-immobile water type nonequilibrium formulation for solute transport. Two example problems are given to illustrate the potentially important effects of preferential flow on the simulation results. One application concerns pesticide transport in a tile-drained field for which only limited data were available for model calibration. A second application involves the long-term environmental fate of a radionuclide decay chain released from a mining installation in Amazonia processing ore containing natural occurring radioactive materials.

INTRODUCTION

Despite significant advancements during the past several decades, accurate simulation of fluid flow and contaminant transport in the subsurface remains a challenge in many cases. This is especially true when trying to predict transport in natural field systems, which can be extremely heterogeneous at a range of scales. These heterogeneities often lead to preferential or nonequilibrium flow processes that are very difficult to capture macroscopically with standard model formulations. The standard models generally are based on the classical Richards equation for flow in variably-saturated media and the equilibrium advection dispersion equation for solute transport. A large number of processes are known to contribute to preferential flow at the field scale. These include the rapid movement of water and dissolved constituents through soil macropores or rock fractures, unstable or gravity-dominated flow caused by soil textural changes or water repellency, and funneling of water along inclined textural boundaries. Recent reviews of preferential flow and transport processes and related modeling approaches are given by Hendrickx and Flury [2001], Simunek et al. [2003] and Gerke [2006].

A variety of physical and chemical nonequilibrium models have been formulated over the years in attempts to parameterize preferential flow. In this paper we briefly review the classical formulations for flow and transport in variably-saturated media, and then provide an overview of available dual-porosity, dual-permeability and related formulations for modeling nonequilibrium or preferential flow and transport in the subsurface. We also show two example applications. One

application concerns the transport of a pesticide (bentazone) in a large-scale tile-drained field for which only limited data were available for model calibration [Boivin et al., 2006]. The second application involves the long-term environmental fate and transport of a radionuclide decay chain ($^{238}U \rightarrow {}^{234}U \rightarrow {}^{230}Th \rightarrow {}^{226}Ra \rightarrow {}^{210}Pb$) released from a mining installation in Amazonia processing ore containing natural occurring radioactive materials (NORMs).

CLASSICAL DESCRIPTIONS FOR FLOW AND TRANSPORT

Predictions of water and solute movement in the vadose zone are typically made using the classical Richards equation for flow in unsaturated porous media and the advection-dispersion equations for solute movement. For a one-dimensional vertical profile, these equations are as follows

$$\frac{\partial \theta(h)}{\partial t} = \frac{\partial}{\partial x}\left(K(h)\frac{\partial h}{\partial x} - K(h) \right) \tag{1}$$

$$\frac{\partial \theta c}{\partial t} + \frac{\partial \rho s}{\partial t} = \frac{\partial}{\partial x}\left(\theta D \frac{\partial c}{\partial x} \right) - \frac{\partial qc}{\partial x} - \phi \tag{2}$$

respectively, where θ is the volumetric water content, h is the soil water pressure head, t is time, x is distance from the soil surface downward, K is the unsaturated hydraulic conductivity as a function of h or θ, c is the solution concentration, ρ is the solid phase bulk density, s is the adsorbed (solid phase) concentration, ϕ is a general source-sink term, q is the volumetric fluid flux density given by Darcy-Buckingham's law as

$$q = -K(h)\frac{\partial h}{\partial x} + K(h) \tag{3}$$

and D is the dispersion coefficient given by

$$D = D_o \tau + \lambda |v| \tag{4}$$

in which D_o is the molecular or ionic diffusion coefficient, τ is the tortuosity factor, λ is the dispersivity, and v ($=q/\theta$) is the average pore-water velocity. For simplicity all of the flow and transport equations discussed in this paper are formulated for one-dimensional vertical flow through the vadose zone. Similar equations can be formulated for two- or three-dimensional problems [Simunek et al., 1999; Simunek and van Genuchten, 2006].

The hydraulic (constitutive) relationships $\theta(h)$ and $K(h)$ needed in applications of Eq. (1) are described here using the functions [van Genuchten, 1980]

$$\theta(h) = \theta_r + \frac{\theta_s - \theta_r}{[1 + |\alpha h|^n]^m} \qquad (m = 1 - 1/n) \tag{5}$$

$$K(h) = K_s \sqrt{S_e}\left[1 - (1 - S_e^{1/m})^m \right]^2 \tag{6}$$

where θ_r and θ_s denote the residual and saturated water contents, respectively, α and n are empirical shape factors, K_s is the saturated hydraulic conductivity, and S_e is effective fluid saturation given by

$$S_e(h) = \frac{\theta - \theta_r}{\theta_s - \theta_r} \tag{7}$$

For all of the solute transport applications discussed in this study we assume linear equilibrium partitioning between the solution and adsorbed phases (i.e., $s = K_d\, c$), in which case the transport equation reduces to

$$\frac{\partial \theta R c}{\partial t} = \frac{\partial}{\partial x}\left(\theta D \frac{\partial c}{\partial x} \right) - \frac{\partial q c}{\partial x} \tag{8}$$

where R is the retardation factor:

$$R = 1 + \frac{\rho K_d}{\theta} \tag{9}$$

The above flow and transport formulations are relatively standard in that they have been used for the past several decades in various forms, simplifications or extensions in a large number of research and engineering applications. The equations typically predict uniform flow and transport processes in the subsurface that ignore the presence of physical non-equilibrium and preferential flow. We next briefly review possible formulations that may be used to describe preferential flow in soils and groundwater.

DUAL-POROSITY/PERMEABILITY FORMULATIONS

Preferential flow in macroporous soils and fractured rocks can be described using a variety of dual-porosity or dual-permeability models. Figure 1 shows schematics of possible equilibrium and physical nonequilibrium models for water flow and solute transport [Simunek and van Genuchten, 2008]. Figure 1a pertains to equilibrium flow and transport. The mobile-immobile nonequilibrium (Fig. 1b), dual-porosity (Fig. 1c) and dual-permeability (Fig. 1d) models typically assume that the porous medium consists of two overlapping but interacting pore regions, one associated with the inter-aggregate, macropore, or fracture pore system, and one comprising the micropores (or intra-aggregate pores) inside soil aggregates or the rock matrix. Dual-porosity models assume that water in the matrix is stagnant, while the more complex dual-permeability models also consider water flow within the soil or rock matrix.

In the dual-permeability approach, Richards equations are applied to both the macropore or fracture pore system and the matrix region. The flow equations for the fracture (subscript *f*) and matrix (subscript *m*) pore systems in that case are given by

$$\frac{\partial \theta_f(h_f)}{\partial t} = \frac{\partial}{\partial x}\left[K_f(h_f) \frac{\partial h_f}{\partial x_j} - K(h_f) \right] - \frac{\Gamma_w}{w} \tag{10a}$$

$$\frac{\partial \theta_m(h_m)}{\partial t} = \frac{\partial}{\partial x}\left[K_m(h_m) \frac{\partial h_m}{\partial x} - K_m(h_m) \right] + \frac{\Gamma_w}{1 - w} \tag{10b}$$

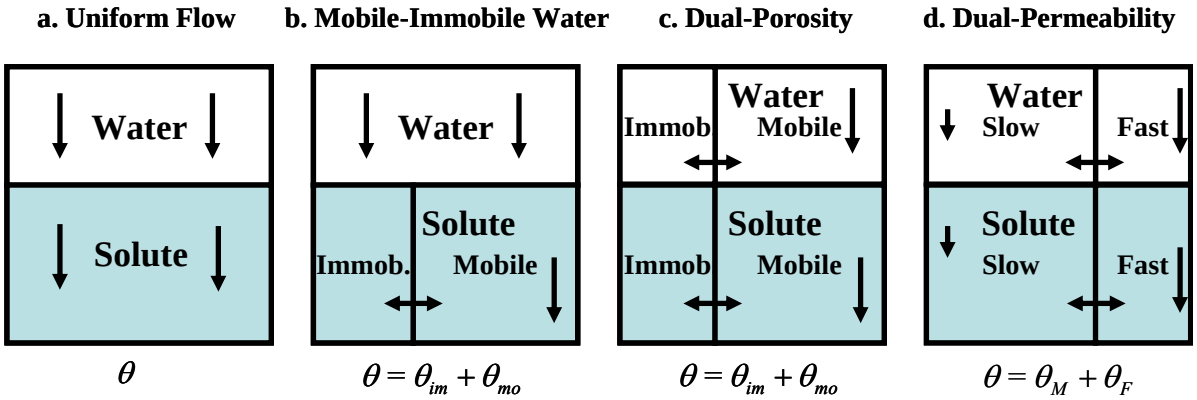

Figure 1. Conceptual models for equilibrium and preferential flow of water and solutes. In the schematics, θ is the water content, θ_{mo} and θ_{im} in (b) and (c) are water contents of the mobile and immobile flow regions, respectively, and θ_F (=$w\theta_f$) and θ_M (=(1-w)θ_m) in (d) are water contents of the matrix and macropore (fracture) regions, respectively (Simunek and van Genuchten, 2008).

respectively, where w is the ratio of the volumes of the fracture domain and the total porous medium. Different dual-permeability formulations arise depending upon how water and solute movement in the fractures and the matrix is modeled, and how water and solutes in the matrix and fracture regions are allowed to interact through the exchange term Γ_w [Gerke and van Genuchten, 1993a; Jarvis, 1999; Simunek et al., 2003]. In previous work we used a simple linear driving force between the matrix and fracture regions based on discretization of Darcy-Buckingham's law for horizontal flow as follows [Gerke and van Genuchten, 1993a]:

$$\Gamma_w = \alpha_w (h_f - h_m) \tag{11}$$

in which α_w is a first-order mass transfer coefficient for flow. An expression for α_w can be derived when the fractured or macroporous porous medium is assumed to have an idealized geometry consisting of well-defined (e.g., rectangular or spherical) matrix blocks, in which case [Gerke and van Genuchten, 1993b]:

$$\alpha_w = \frac{\beta_a \gamma_w K_a(h)}{a^2} \tag{12}$$

where β_a is a dimensionless geometry-dependent coefficient, a is the characteristic length of the matrix structure (e.g., half of the fracture spacing, or the radius of spherical aggregates), γ_w is a dimensionless scaling coefficient, and K_a is the effective hydraulic conductivity of the fracture-matrix interface. Gerke and van Genuchten [1993b] evaluated this conductivity as

$$K_a = \frac{[K_a(h_m) + K_a(h_f)]}{2} \tag{13}$$

Alternative expressions for the exchange term Γ_w and K_a have been suggested by, among others, Zimmerman et al. [1993]) and Köhne et al. [2004].

Analogous to Eqs. (10a,b), the dual-permeability formulation for solute transport is based on advection-dispersion type equations for transport in both the fracture and matrix regions as follows (Gerke and van Genuchten, 1993a):

$$\frac{\partial \theta_f R_f c_f}{\partial t} = \frac{\partial}{\partial z}\left(\theta_f D_f \frac{\partial c_f}{\partial z} \right) - \frac{\partial q_f c_f}{\partial z} - \phi_f - \frac{\Gamma_s}{w} \tag{14a}$$

$$\frac{\partial \theta_m R_m c_m}{\partial t} = \frac{\partial}{\partial z}\left(\theta_m D_m \frac{\partial c_m}{\partial z} \right) - \frac{\partial q_m c_m}{\partial z} - \phi_m + \frac{\Gamma_s}{1-w} \tag{14b}$$

where the subscripts f and m as before refer to the fracture and matrix pore regions, respectively, and Γ_s is the mass transfer term for solute exchange between the two regions:

$$\Gamma_s = \alpha_s (1-w)\theta_m (c_f - c_m) + \Gamma_w c^* \tag{15}$$

in which α_s is a first-order mass transfer coefficient for solute. Equation (15) shows that solute exchange between the two liquid regions is modeled as the sum of an apparent first-order diffusion process and advective transport, with c^* being equal to c_f when $\Gamma_w>0$ (advective transfer from the fracture to the matrix region) and c_m when $\Gamma_w<0$ (advective transfer back to the fractures).

The above dual-permeability formulation presents a potentially very powerful model for simulating preferential flow and transport processes in the subsurface. Example applications of dual-permeability models are given by Pot et al. [2005], Kodesova et al. [2005] and Köhne et al. [2006], among others. While relatively complicated mathematically, the complexity is merely a reflection of the complicated nature in which preferential flow occurs, and the many physical and chemical processes that are known to contribute to preferential flow. And while much has been learned over the years about preferential flow, the dual-permeability models still provide a very simplified mathematical description of the processes involved.

When vertical water flow in matrix is ignored, and hence also no vertical advective transport occurs in the matrix, the above dual-permeability formulations for water and solute reduce to those for dual-porosity models (Fig. 1c). Models of this type further reduce to the more classical two-region mobile-immobile water type physical nonequilibrium transport models (Fig. 1b) when no water is allowed to exchange between the fracture and matrix regions (i.e., $\Gamma_w = 0$). Lateral advective solute exchange between the fracture and matrix regions is then also neglected, but diffuse transfer will continue. Physical nonequilibrium models of this type are discussed in more detail in the next section.

Application of dual-permeability models such as Eq. (10a,b) typically require two water retention functions, $\theta(h)$, one for the matrix and one for the fracture pore system, and two or three conductivity functions in terms of their local pressure heads, i.e., $K_f(h_f)$ for the fracture network, $K_m(h_m)$ for the matrix, and possibly a separate conductivity function $K_a(h_a)$ for the fracture/matrix interface as embedded in the exchange term, Γ_w [Gerke and van Genuchten, 1993a]. Of these functions, K_f is determined primarily by the structure of the fracture pore system (i.e., the size, geometry and continuity of the fractures, and possibly the presence of fracture or macropore coatings). Similarly, K_m is determined by the hydraulic properties of single matrix blocks, and the degree of hydraulic contact between adjacent matrix blocks during unsaturated flow. Such information, unfortunately, is seldom available in practice. For these reasons a number of

simplifications are often invoked, such as instantaneous hydraulic equilibration between the fracture and matrix pore systems.

TWO-REGION PHYSICAL NONEQUILIBRIUM MODELS

To avoid over-parameterization of the governing equations, one simplifying approach is to assume instantaneous hydraulic equilibration between the fracture and matrix regions such that $h_f = h_m$ (= h). In that case the coupling term Γ_w can be eliminated from Eqs. (10a,b) to recover Eq. (1), but now with composite hydraulic properties of the form

$$\theta(h) = w\theta_f(h) + (1-w)\theta_m(h) \tag{16a}$$

$$K(h) = wK_f(h) + (1-w)K_m(h) \tag{16b}$$

Many studies have used composite hydraulic properties of the type given by Eqs. (16a,b), especially for the hydraulic conductivity function [Peters and Klavetter, 1988; Durner, 1994; Mohanty et al., 1997, Zurmühl and Durner, 1996; Vogel and Cislerova, 1998; de Vos et al., 1999]. While still leading to uniform flow, models using such composite media properties do allow for faster flow and transport during conditions near saturation, and as such may provide more realistic simulations of field data than the standard approach using unimodal hydraulic properties. In soils, the two parts of the conductivity curves may be associated with soil structure (near saturation) and soil texture (at lower negative pressure heads).

Very much consistent with Eqs. (16a,b) are composite hydraulic functions as described with the model of Durner [1994] as follows

$$S_e(h) = \frac{\theta(h)-\theta_r}{\theta_s-\theta_r} = \frac{w_1}{[1+|\alpha_1 h|^{n_1}]^{m_1}} + \frac{w_2}{[1+|\alpha_2 h|^{n_2}]^{m_2}} \tag{17}$$

$$K(S_e) = K_s \frac{\left(w_1 S_{e_1} + w_2 S_{e_2}\right)^l \left\{ w_1\alpha_1[1-(1-S_{e_1}^{1/m_1})^{m_1}] + w_2\alpha_2[1-(1-S_{e_2}^{1/m_2})^{m_2}] \right\}^2}{\left(w_1\alpha_1 + w_2\alpha_2\right)^2} \tag{18}$$

where w_i are the weighting factors for the two overlapping regions, and α_i, n_i, and m_i are empirical parameters of the separate hydraulic functions (i =1,2, …). An example of composite retention and hydraulic conductivity functions based on Eqs (17) and (18) is shown in Fig. 2 for the following set of parameters: θ_r=0.00, θ_s=0.50, α_1=0.01 cm^{-1}, n_1=1.50, l=0.5, K_s=1 cm d^{-1}, w_1=0.975, w_2=0.025, α_2=1.00 cm^{-1}, and n_2=5.00. The fracture domain in this case represents only 2.5% of the entire pore space, but accounts for almost 90% of the hydraulic conductivity close to saturation.

Measurements of the composite (fracture plus matrix) hydraulic properties are greatly facilitated by the use of tension infiltrometers. An advantage of tension infiltrometry is that negative soil water pressures at the soil-infiltrometer interface can be maintained very close to zero, and that they can be decreased in small steps to yield well-defined functions near saturation [e.g., Mohanty et al., 1997].

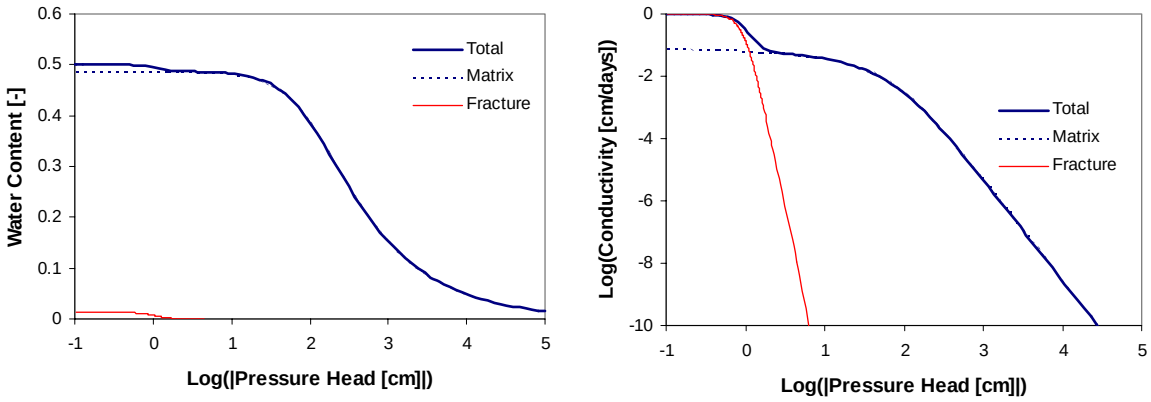

Figure 2. Bimodal (composite) water retention (left) and hydraulic conductivity (right) functions as described with the model of Durner [1994].

The use of composite hydraulic functions such as those shown in Fig. 2 is consistent with field measurements suggesting that the macropore conductivity of soils at saturation is generally about one to two orders of magnitude larger than the matrix conductivity at saturation, depending upon texture. These findings were recently confirmed by Schaap and van Genuchten, 2006) using a detailed neural network analysis of the UNSODA unsaturated soil hydraulic database [Leij et al., 1996; Nemes et al., 2001]. The analysis revealed a relatively sharp decrease in the conductivity away from saturation and a slower decrease afterwards. Schaap and van Genuchten (2005) suggested an improved composite function for $K(h)$ to account for the effects of macropores near saturation as follows:

$$K(h) = \left(\frac{K_s}{K_m(h)} \right)^{R(h)} K_m(h) \tag{19}$$

where

$$R(h) = \begin{cases} 0 & h < -40 \text{ cm} \\ 0.2778 + 0.00694h & -40 \le h < -4 \text{ cm} \\ 1 + 0.1875h & -4 \le h \le 0 \text{ cm} \end{cases} \tag{20}$$

and where $K_m(h)$ is the traditional hydraulic conductivity function for the matrix as given by Eq. (6) but with a different exponent for the tortuosity term (the square root term) in Eq. (6). Equations (19) and (20) were found to produce very small systematic errors between the observed (UNSODA) and calculated hydraulic conductivities across a wide range of pressure heads between saturation and -150 m. While the macropore contribution was found to be most significant between pressure heads 0 and -4 cm, its influence on the conductivity function extended to pressure heads as low as -40 cm (Eq. 20).

If Eq. (1) is used in conjunction with composite hydraulic functions such as those given by Eqs (16a,b) or Eqs. (19) and (20), the solute transport equation for nonequilibrium flow will no longer contain an advection term in the solute exchange term between the matrix and fracture regions. The transport equations for nonequilibrium transport reduce then to a relatively standard dual-porosity formulation which assumes that the liquid phase can be partitioned into mobile, $\theta_{mo} = w\theta_f$, and

immobile, $\theta_{im} = (1\text{-}w)\theta_f$, regions, with advective-dispersive transport being restricted to the mobile region as follows [van Genuchten and Wagenet, 1989]:

$$\frac{\partial \theta_{mo} R_{mo} c_{mo}}{\partial t} = \frac{\partial}{\partial x}\left(\theta D \frac{\partial c_{mo}}{\partial x} \right) - \frac{\partial q c_{mo}}{\partial x} - \alpha_s (c_{mo} - c_{im}) - \phi_{mo} \tag{21a}$$

$$\frac{\partial \theta_{im} R_{im} c_{im}}{\partial t} = \alpha_s (c_{mo} - c_{im}) - \phi_{im} \tag{21b}$$

in which

$$R_{mo} = 1 + \frac{f \rho K_d}{\theta_{mo}} \qquad R_{mo} = 1 + \frac{(1-f) \rho K_d}{\theta_{im}} \tag{22}$$

where the subscripts *mo* and *im* refer to the mobile (macropore or fracture) and immobile (matrix) regions, respectively, *f* is the dimensionless fraction of sorption sites in contact with mobile water, and α_s is the solute mass transfer coefficient between the two regions. Please note that the exchange term in Eq. (21a,b) does not contain the mobile water content, θ_{mo}, such as was the case with Eq. (15). This was done to keep the same model formulation as used previously by van Genuchten and Wierenga [1976] and van Genuchten and Wagenet [1989].

The totality of Eqs. (1), (16a,b) and (21a,b) provide a very convenient and parsimonious description of nonequilibrium transport in soils and groundwater. One challenge still is the definition of the mass transfer coefficient, α_s. In earlier work [van Genuchten and Dalton, 1986; Gerke and van Genuchten, 1993b] we related this value to geometric properties of the fractures or matrix. While useful in concept, field soils are generally too complicated for simplified geometric analyses. Moreover, evidence exists that the mass transfer coefficient α_s decreases with the scale of the transport problem. Based on analysis of previously published laboratory and intermediate field-scale experiments, Maraqa [2001] found that α_s is inversely related to the residence time of the contaminant in the system as follows:

$$\alpha_s = a t_r^{-b} \tag{23}$$

where α_s is given in 1/hours, t_r is the residence time in hours ($t_r = LR/v_m$ in which *L* is the length of the transport domain and v_m the mobile region pore-water velocity given by q/θ_{mo}), *a* was 0.012 for stony soils, 0.26 for aggregated media, and 0.95 for non-aggregated media; while *b* was found to be in the range 0.73 to 0.88. Equation (22) shows that α_s is a scale-dependent parameter, roughly inversely proportional (exactly if *b*=1) to the scale of an experiment. Scale dependency has long been known for several transport parameters such as the longitudinal dispersivity, λ, which is generally assumed to increase with the length of the transport domain [e.g., Anderson, 1984]. Scale dependency may well exist also macroscopically for the matrix diffusion coefficient [Liu et al., 2004].

The scale dependency of the mass transfer coefficient also makes sense intuitively if one accepts the notion that some degree of nonequilibrium always will be present during transport in naturally heterogeneous media, with the degree of non-equilibrium being controlled by new heterogeneities continuously being encountered as the transport domain increases (e.g., Pachepsky, 2008). This notion can be demonstrated by placing Eqs. (21a,b) in dimensionless form for steady-state flow in a homogeneous medium as follows [van Genuchten and Wagenet, 1989]:

$$\beta R\frac{\partial c_1}{\partial T}+(1-\beta)R\frac{\partial c_2}{\partial T}=\frac{1}{P}\frac{\partial^2 c_1}{\partial z}-\frac{\partial c_1}{\partial x}-\omega(c_1-c_2)-\phi_{mo}^{*} \tag{24a}$$

$$(1-\beta)R\frac{\partial c_2}{\partial T}=\omega(c_1-c_2)-\phi_{im}^{*} \tag{24b}$$

where

$$T=\frac{qt}{\theta L}\qquad X=\frac{x}{L}\qquad c_1=\frac{c-C_i}{C_o-C_i}\qquad c_2=\frac{c-C_i}{C_o-C_i} \tag{25a,b,c}$$

$$\beta=\frac{\theta_{mo}+\rho f K_d}{\theta+\rho K_d}=\frac{\theta_{mo}R_{mo}}{\theta R}\qquad \omega=\frac{\alpha L}{q}\qquad P=\frac{qL}{\theta_{mo}D} \tag{25d,e,f}$$

in which L is the length of the transport domain, T and z are dimensionless time (often referred to as pore volume) and distance, respectively, C_i and C_o are the initial and inlet (at x=0) concentrations (assumed to be constants here), β accounts for the fraction of the porous medium containing the mobile liquid and the sorption sites in equilibrium with mobile liquid ($0 \le \beta \le$ l), ω is the dimensionless mass transfer coefficient, and ϕ_{mo}^{*} and ϕ_{im}^{*} are dimensional source-sink terms.

If the degree of nonequilibrium of the medium would not change with the spatial scale of the transport problem, then the dimensionless mass transfer ω in Eq. (24b) would become a constant independent of scale. Constancy of ω independent of scale (or the resident time) would imply an inverse relationship between α_s and L, consistent with Eq. (23) if b = -1. Assuming b = -1 and using the inventoried data of Maraqa [2001] for both aggregated and intermediate field-scale data suggests the following approximate relationship for α_s:

$$\alpha_s=\frac{q}{8L\theta\beta R} \tag{26}$$

which is now independent of the units used for α_s, q and L. The applicability of Eq. (26) definitely needs further testing in future studies, especially the constant 8 in the denominator of Eq. (26).

APPLICATIONS

We now briefly summarize two applications of the physical nonequilibrium models. One application (Boivin et al., 2006) concerns pesticide transport in a large-scale tile-drained field for which only limited data were available for model calibration [Boivin et al., 2006]. A second application [Pontedeiro et al., 2009] involves the long-term transport of a radionuclide decay chain released from a conventional mining installation in Amazonia processing ore containing natural occurring radioactive materials.

Example 1. Pesticide Transport in a Tile-Drained Field This example concerns the subsurface transport of the herbicide bentazone in a tile-drained agricultural field in northeastern France. The field consisted of two separate experimental sites (Fig. 3): Bouzule-1 made up of mostly silt loam, and Bouzule-2 consisting of relatively fine-textured silty clay. Here we consider only transport at the Bouzule-2 site, which was equipped with a subsurface tile drain system (0.05 m diameter), with tiles at an average depth of 0.9 m and a drain spacing of 8 m. Precipitation rates and other meteorological variables were recorded at a weather station approximately 2 km from the field site.

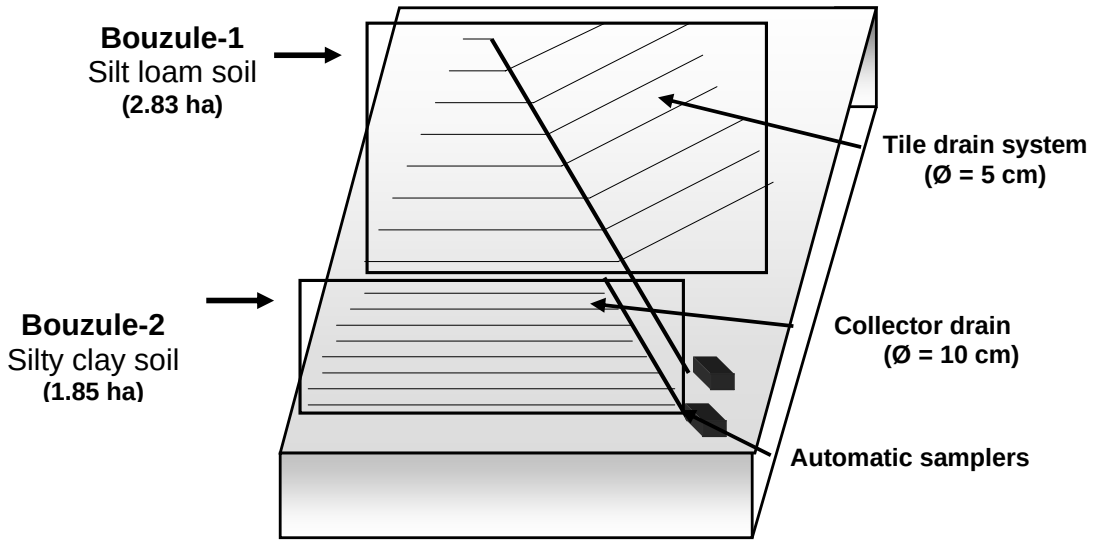

Figure 3. Layout of the tile drainage systems at the Bouzule field sites [after Boivin et al., 2006].

Bentazone was sprayed onto the Bouzule-2 site on March 11, 2002. We used the HYDRUS-2D software package [Simunek et al., 1999] to simulate the subsurface transport of this pesticide for a period of 100 days after application. The governing equations were exactly the same as before, except for their extension to two dimensions [Boivin et al., 2006]. In the study we assumed isotropic media, included provisions for root water uptake, but neglected pesticide degradation since laboratory experiments indicated little or no degradation over time periods pertinent to the field experiments. We refer to Boivin et al. [2006] for a detailed discussion of the field experiments, the invoked flow and transport models, and the data used for the simulations.

Figure 4 shows the unstructured finite element mesh used in the simulations. The grid was stratified in accordance with observed soil profile layering. Boundary conditions included no-flow boundaries along the sides, atmospheric conditions at the soil surface (i.e., daily precipitation and

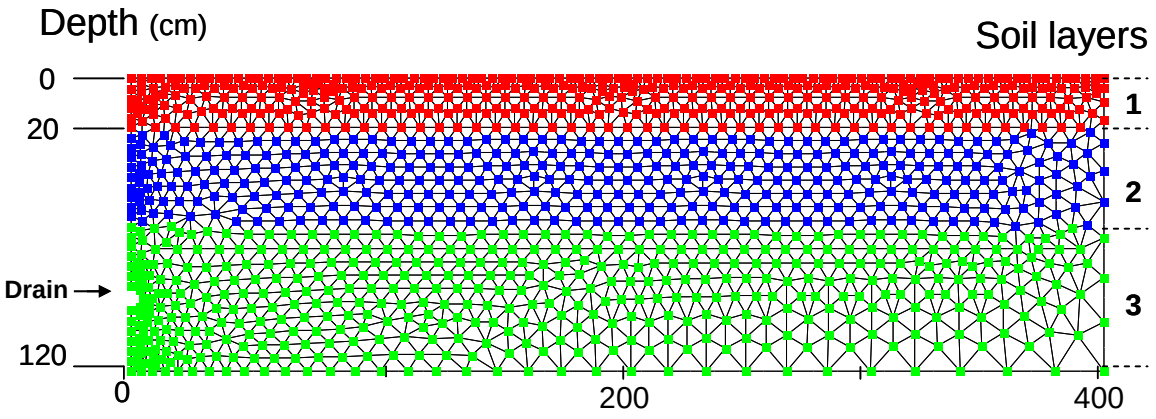

Figure 4. Unstructured finite element grid used for the layered transport domain representing half the drain spacing of the simulated Bouzule-2 silty clay site. The grid consisted of 2298 triangular elements and 1237 nodes [Boivin et al., 2005].

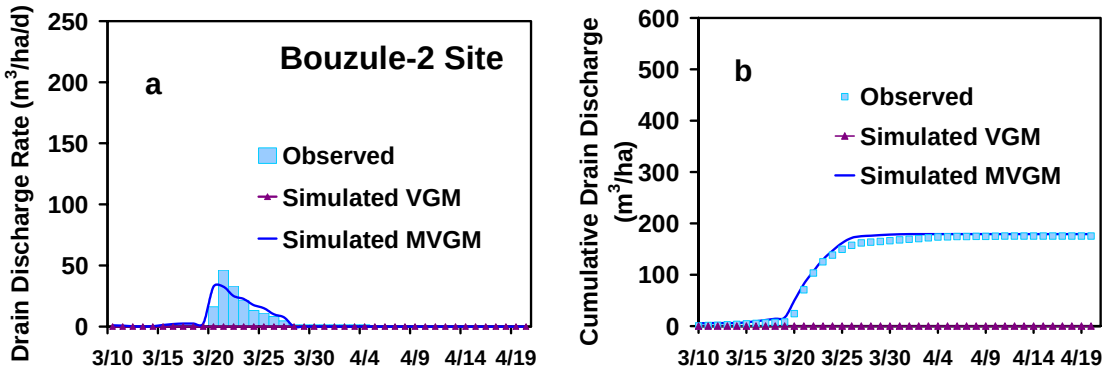

Figure 5. Observed and simulated instantaneous (a) and cumulative (b) tile drain discharge rates. Flow simulations were carried out with the standard (VGM) hydraulic functions given by Eqs. (5) and (6), and the modified MVGM) functions given by Eqs. (27) and (28) [Boivin et al., 2005].

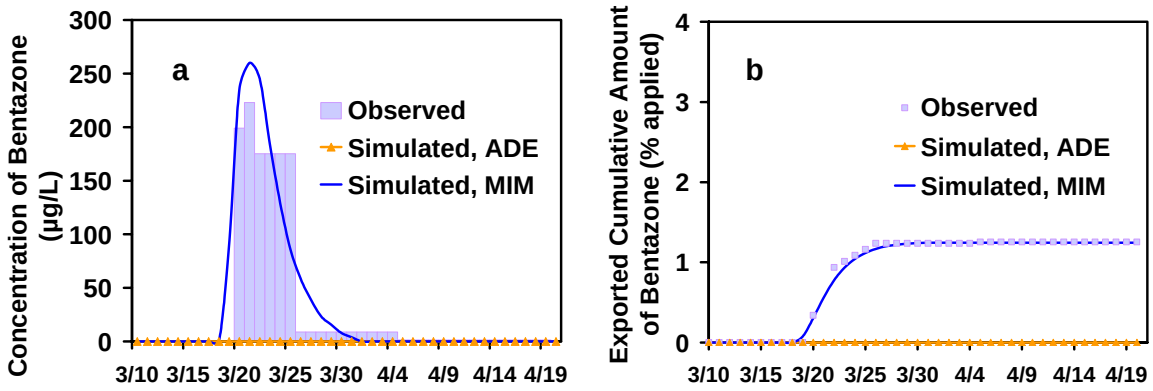

Figure 6. Observed and simulated bentazone concentrations in the drainage water (a) and cumulative amount of bentazone exported (b) for the Bouzule-2 silty clay site. Solute transport simulations were carried out with both the equilibrium advection-dispersion equation (ADE) and the mobile-immobile (MIM) physical non-equilibrium transport model [Boivin et al., 2005].

evaporation rates), a free drainage bottom boundary conditions, and a seepage face at the tile drain (which implies that the drains function only when the surrounding soil is saturated). Initial simulations started on January 10, 2002, about 2 months before the pesticide application, with an equilibrium pressure head profile so as to obtain realistic soil water contents in the profile at the time of the pesticide application.

Observed and measured tile drainage discharge rates and concentrations, as well as cumulative amounts, are shown in Figs. 5 and 6. Observed data (Fig. 6a) indicated very high pesticide concentrations in the drainage water (a maximum concentration of 223 µg L^{-1}), substantially higher than the limit of 0.1 µg L^{-1} set by the European Union for pesticide concentrations in groundwater [Focus Leaching Modelling Workgroup, 1995], and also above 3 µg L^{-1} used by the U.S. Environmental Protection Agency for the maximum contaminant level for bentazone [USEPA,

2004]. Evidence of preferential flow at this site, especially during the normally relatively wet spring and summer seasons, was demonstrated previously by several other experiments conducted with a bromide tracer and the pesticide metolachlor (Novak et al., 2003)

HYDRUS-2D simulations using the traditional (VGM) hydraulic functions given by Eqs. (5) and (6) were found to severely underestimate the observed drain discharge rates (Fig. 5). K_s values obtained from laboratory experiments did not account for the influence of drying cracks at the site, and thus substantially underestimated actual K_s values in the field, especially during spring and summer when drying developed in especially the soil surface horizon. To account for these cracks, the modified (MVGM) soil hydraulic functions of Vogel et al. [2000] were used to mimic the effects of preferential. These functions provide yet another way to account for the effects of macroporosity on variably-saturated flow, similarly as was shown in Fig. 2. The hydraulic functions of Vogel et al. [2000] are given by

$$\theta(h) = \begin{cases} \theta_r + \dfrac{\theta_m - \theta_r}{(1+|\alpha h|^n)^m} & h < h_s \\ \theta_s & h \geq h_s \end{cases} \tag{27}$$

$$K(h) = \begin{cases} K_k \left(\dfrac{\theta - \theta_r}{\theta_k - \theta_r} \right)^l \left[\dfrac{1 - F(\theta)}{1 - F(\theta_k)} \right]^2 & h \leq h_k \\ K_k + \dfrac{(h - h_k)(K_s - K_k)}{h_s - h_k} & h_k < h < h_s \\ K_s & h \geq h_s \end{cases} \tag{28}$$

where l is a tortuosity factor in the conductivity term (assumed to be 0.5 in Eq. (6)), and

$$F(\theta) = \left[1 - \left(\frac{\theta - \theta_r}{\theta_m - \theta_r} \right)^{1/m} \right]^m \tag{29}$$

Equation (27) introduces a very small air entry value in $\theta(h)$ near saturation by replacing θ_s in Eq. (5) with a fictitious parameter θ_m slightly larger than θ_s. While this modification has little effect on the retention curve, the effect on the shape and value of the hydraulic conductivity function can be considerable, especially for fine-textured soils [Vogel et al., 2000; Schaap and van Genuchten, 2005]. Equation (28) assumes that the predicted hydraulic conductivity function is matched to a measured value of the conductivity, $K_k=K(\theta_k)$, at some water content $\theta_k \leq \theta_s$ where $K_k \leq K_s$. The conductivity function is then assumed to increase linearly between h_k and saturation to account for macropore flow. Only a few of the hydraulic parameters in Eqs (27) and (28) were obtained from direct measurements (notably θ_s, θ_s and K_k). Others (α and n) were estimated from soil texture using the Rosetta pedotransfer functions [Schaap et al., 1996], while K_s and h_k were calibrated against the observed drainage data.

Using Eqs. (27) and (28) with K_s values up to about 20 times the measured K_k values for some of the layers, did lead to much more accurate simulations of the drain discharge rate during the spring of 2002. However, we acknowledge that it is very unlikely that the selected combination of K_k values in the simulations represented a single unique description of the macropore flow process at the site.

Figure 6 shows that the concentrations and amounts of pesticide discharged from the tile-drainage field were severely underestimated using the equilibrium (ADE) model. An excellent fit could be obtained with the mobile-immobile (MIM) physical nonequilibrium model upon calibration of the mass transfer coefficient, α_s, and equating the immobile water content, θ_r, to the residual water content, θ_r for all three layers. A single α_s value of 0.027 d^{-1} for all three layers produced excellent agreement with the measured concentrations (Fig. 5a) as well as with the total amount of bentazone exported with the drainage water. The fitted value of 0.027 d^{-1} for a_s was well within the range of values used by Maraqa [2001] for intermediate-scale field studies, but slightly lower than most laboratory studies analyzed by Maraqa [2001], including α_s values predicted with Eq. (26).

The pesticide study shows that a limited amount of input data could be used to successfully simulate drain discharge rates and chemical concentrations using an equilibrium flow model with composite hydraulic conductivity function, and the mobile-immobile physical nonequilibrium model. The modified soil hydraulic functions in this example apparently provided sufficient flexibility to permit accurate simulations at the site.

Example 2. Radionuclide Transport from a NORM Mining Waste Site In this example we investigate the environmental fate of a radionuclides being released from a still operating conventional mining installation in Amazonia processing ore containing natural occurring radioactive materials (NORMs). The study was initially motivated by Brazilian regulations requiring a performance assessment of the disposal facility using a leaching and off-site transport scenario. We used for our analysis the HYDRUS-1D software package [2005] to predict the long-term transport of radionuclides moving vertically through both the landfill and then laterally in groundwater until a well 100 m downgradient from the site. The analysis was limited to the radionuclide decay chain $^{238}U \rightarrow {}^{234}U \rightarrow {}^{230}Th \rightarrow {}^{226}Ra \rightarrow {}^{210}Pb$. We refer to Pontedeiro et al. [2009] for a more detailed description of the site, the hydraulic and transport parameters used in the numerical analyses, and the modeling results.

For the calculations we assumed a 6-m thick homogeneous waste layer (overlain by a negligibly thin layer of local soil), and a 5-m thick unsaturated zone. Radionuclides leaching vertically from the vadose zone were assumed to mix with laterally moving groundwater. The long-term average recharge rate at the site was estimated to be 657 mm/y. This recharge rate was used as a surface flux boundary condition for steady-state simulations of water and dissolved radionuclides flowing through the site and into groundwater. The mixing process between vadose zone recharge water and laterally moving groundwater was described using the EPA mixing zone model [USEPA, 1996]. Initial radionuclide concentrations of the waste layer were estimated to be 71 Bq/g for ^{238}U and ^{234}U, 67 Bq/g for ^{230}Th, 63 Bq/g for ^{226}Ra and 4.8 Bq/g for ^{210}Pb.

Transport calculations for this problem were previously carried out by Pontedeiro et al. [2009] for both a best-case scenario assuming equilibrium transport in a fine-textured (clay) subsurface, and a worst-case scenario with preferential flow in a very coarse-textured (sand) subsurface using the mobile immobile physical nonequilibrium model. For those calculations we first used measured or estimated hydraulic and transport properties of the slags and the local soil, a red saprolite known as Belterra clay [Truckenbrodt and Kotschoubey, 1981, Belk et al., 2008]. The calculations involved very high K_d

values, taken from ISAM [1999], and hence retardation factors for the different radionuclides, leading to relatively low transport rates over the assumed 100,000 year simulation period. We subsequently contrasted those simulations with results for a coarse-textured subsurface. Hydraulic properties of the vadose zone below the waste layer were again described with Eqs. (5) and (6), but now using parameters for a sand as predicted with the Rosetta pedotransfer functions [Schaap et al., 1998].

The transport of each radionuclide (subscript *i*) within the radionuclide decay chain was initially modeled using the equilibrium advection-dispersion equation:

$$\frac{\partial \theta R_1 c_1}{\partial t} = \frac{\partial}{\partial x}\left(\theta D \frac{\partial c_1}{\partial x} \right) - \frac{\partial q c_1}{\partial x} - \mu_1 \theta R_1 c_1 \tag{30a}$$

$$\frac{\partial \theta R_i c_i}{\partial t} = \frac{\partial}{\partial x}\left(\theta D \frac{\partial c_i}{\partial x} \right) - \frac{\partial q c_i}{\partial x} + \mu_{i-1} \theta R_{i-1} c_{i-1} - \mu_i \theta R_i c_i \qquad (i = 2,5) \tag{30b}$$

where the μ_i's represents first-order source-sink coupling between consecutive radionuclides within the decay chain, with decay occurring in both the solution and adsorbed phases (accounted for by using retardation factors in the decay terms).

Equations (29a,b) assume equilibrium transport. We also simulated the transport problem assuming mobile/immobile type physical nonequilibrium transport. The governing transport equations for the *i*-th radionuclide in the decay chain are then of the form [see also van Genuchten and Wagenet, 1989]

$$\frac{\partial \theta R_{mo,i} c_{mo,i}}{\partial t} = \frac{\partial}{\partial x}\left(\theta D \frac{\partial c_{mo,i}}{\partial x} \right) - \frac{\partial q c_{mo,i}}{\partial x} - \alpha_s (c_{mo,i} - c_{im,i}) + \mu_{i-1} \theta R_{mo,i-1} c_{mo,i-1} - \mu_i \theta R_{mo,i} c_{mo,i} \tag{30a}$$

$$\frac{\partial \theta R_{im,i} c_{im,i}}{\partial t} = \alpha_s (c_{im,i} - c_{im,i}) + \mu_{i-1} \theta R_{im,i-1} c_{im,i-1} - \mu_i \theta R_{im,i} c_{im,i} \tag{30b}$$

where as before the subscripts *mo* and *im* refer to the mobile and immobile liquid phases. Equations (30a,b) allow simulation of nonequilibrium transport with a minimum of additional transport parameters. Following Nkedi-Kizza et al. [1983], f was set equal to the relative fraction of mobile water (i.e., $f = \theta_m/\theta$), which makes these two parameters numerically equal to the dimensional parameter β given by Eq. (25d). For the analysis we used α_s values recommended by Maraqa [2001] based on Eq. (26) assuming a and b values for non-aggregated media. Estimated values of α_s for the Belterra clay calculations varied between approximately 0.0001 and 0.005 year^{-1}, while those for the sand were approximately 10 to 100 times larger depending upon the soil layer (vadose zone or aquifer) and radionuclide involved. Dispersivities were assumed to be one tenth of the length of each subdomain, while radionuclide half-life data were taken from ICRP [1983].

We first considered equilibrium transport in each of the three media (waste, vadose zone, and groundwater). Calculated concentrations for Belterra clay are shown in Fig. 7. Please note the different scales for the concentrations in these and subsequent figures. Results show that ^{238}U and ^{234}U have by far the highest concentrations at both the bottom of the vadose zone and the well. However, some contribution of ^{230}Th is also clearly present in the leachate from the vadose zone, but not at the well 100 m downgradient from the site.

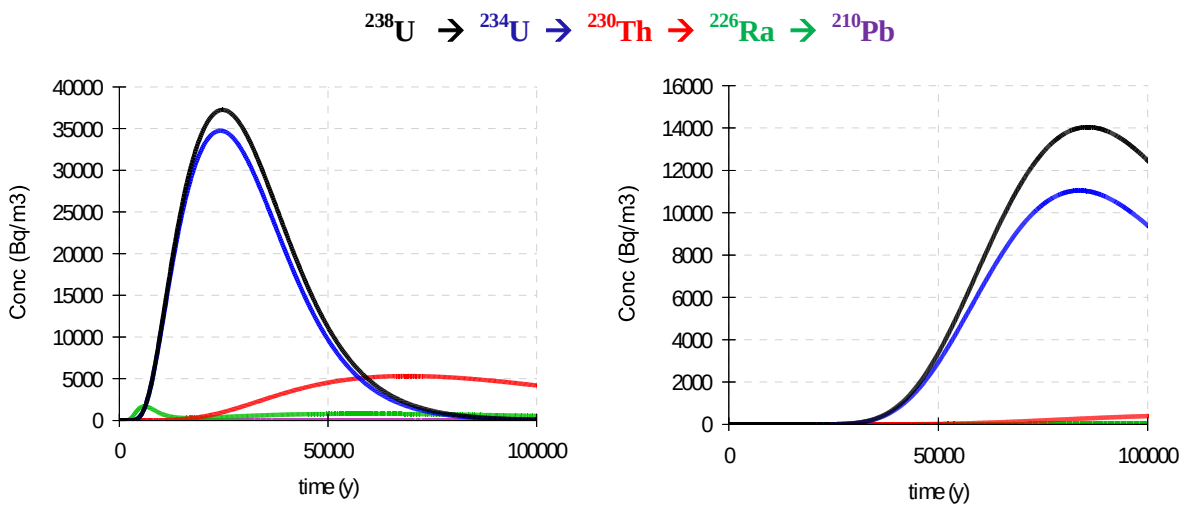

Figure 7. Calculated radionuclide concentrations versus time leaving the vadose zone (left) and at the well (right) assuming equilibrium transport (Belterra clay).

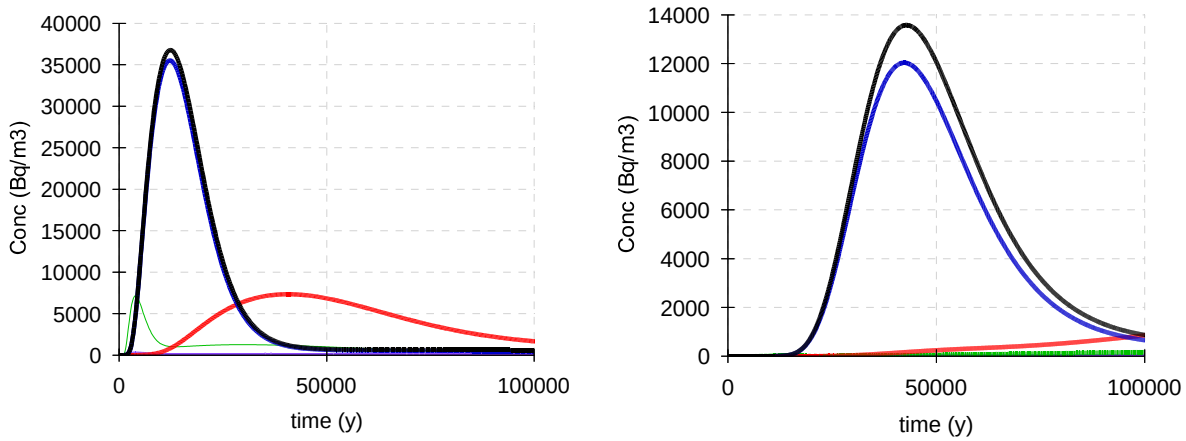

Figure 8. Calculated radionuclide concentrations versus time leaving the vadose zone (left) and at the well (right) assuming nonequilibrium transport (Belterra clay).

Figure 8 presents results when accounting for preferential flow through the waste and the Belterra clay vadose zone and aquifer. Comparing Figs. (7) and (8) shows that the peak concentrations for uranium (having the highest concentrations) are only marginally affected by preferential flow (they are slightly higher for preferential flow simulations). However, the peak concentrations arrive now much earlier at the bottom of the vadose zone and especially at the well (after 43,000 years for preferential flow versus 83,000 years for equilibrium transport). The first radionuclides also arrived much earlier at the well (12,500 years for preferential flow versus 22,000 years for equilibrium transport).

All of the simulations thus far were carried out for Belterra clay, leading to very conservative values for both the hydraulic conductivity (low) and the estimated K_d's (high), thus leading to very low contaminant transport rates. A complementary set of simulations was carried out to show the impact of soil texture on the long-term concentrations. For these simulations we assumed the presence of a very

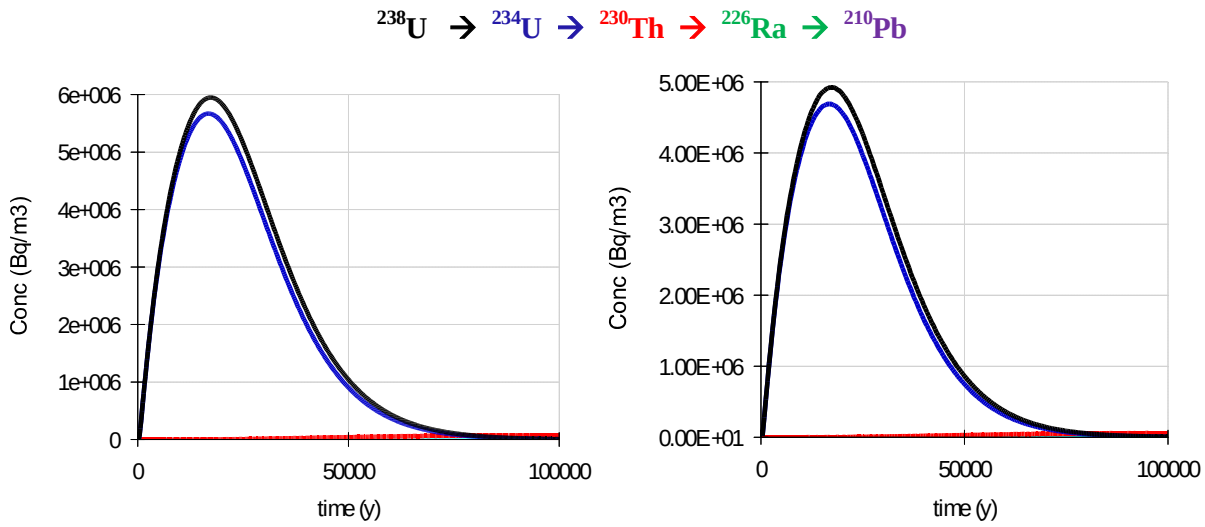

Figure 9. Calculated radionuclide concentrations versus time leaving the vadose zone (left) and at the well (right) assuming equilibrium transport (sand subsurface).

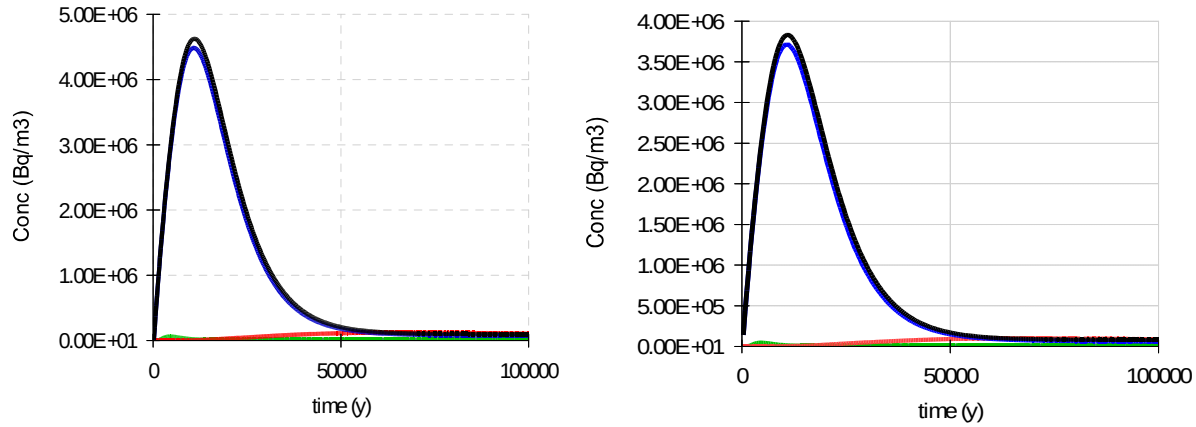

Figure 10. Calculated radionuclide concentrations versus time leaving the vadose zone (left) and at the well (right) assuming nonequilibrium transport (sand subsurface).

coarse-textured subsurface (sand) for both the vadose zone below the waste layer and groundwater, while leaving the physical and chemical properties of the waste layer itself unaltered. K_d were again taken from ISAM (1999), while for the unsaturated hydraulic parameters in Eqs. (1) and (2) we selected typical values for sand using Rosetta.

Results for equilibrium transport from the waste layer through the now sandy subsurface (vadose zone and aquifer) are shown in Fig. 9. As compared to Belterra clay (Fig. 7), the ^{238}U and ^{234}U peaks reached the bottom of the vadose zone much earlier (17,000 versus 24,000 years) with peak concentrations of 5.95 10^6 Bq/m^3, more than 100 times that for the clay soil (3.72 10^4 Bq/m^3). This reflects the much faster transport through the sandy vadose zone. Lateral transport rates through the aquifer were similarly very fast, with the ^{238}U/^{234}U peaks reaching the well 100 m downstream of the site now after only 18,000 years with a peak concentration of 4.92 10^6 Bq/m^3, compared to 85,000 years and a peak concentration of 1.4 10^4 Bq/m^3 for the Belterra clay subsurface.

Finally, Figure 10 shows the effects of preferential flow on the equilibrium results for the sandy subsurface. Comparing the results with those in Fig. 9 for equilibrium transport shows that, similarly as for the Belterra clay subsurface, the peak concentrations were again only marginally higher for the preferential flow scenario (e.g., 4.6 10^6 Bq/m^3 for the sandy vadose zone compared to 3.7 10^4 Bq/m^3 for the clay). The peak concentrations however occurred much earlier, especially at the well (11,000 years for the sand versus 43,000 years for the clay). This shows that both soil texture and preferential flow have a major effect on the radionuclide transport rates.

CONCLUSIONS

In this paper we reviewed a broad range of dual-porosity and dual-permeability formulations for modeling nonequilibrium or preferential fluid flow and contaminant transport in macroporous soils or fractured rock. We focused especially on transport processes in the vadose zone between the soil surface and the groundwater table. One effective modeling approach requiring far fewer hydraulic parameters is to employ composite (dual-porosity type) functions for the unsaturated hydraulic conductivity to account for the separate effects of macropores and micropores, and then to combine this approach with a mobile-immobile water type nonequilibrium formulation for solute transport. The approach was used successfully to simulate pesticide transport in a large-scale tile-drained field for which only limited data were available for model calibration. A second example application involved the long-term environmental the radionuclide decay chain $^{238}U \rightarrow {}^{234}U \rightarrow {}^{230}Th \rightarrow {}^{226}Ra \rightarrow {}^{210}Pb$ being released from a still operating mining installation in Amazonia processing ore containing natural occurring radioactive materials. The two examples show that preferential flow can have a major effect on the simulation results. The physical nonequilibrium formulation used in this study require an estimate of the mass transfer coefficient (α_s) governing diffusive exchange between the fracture and matrix regions of structured media. While some guidance is provided by literature data from laboratory and intermediate scale experiments, more research is needed to determine the exact scale dependency of this parameter, especially for larger scale field applications.

REFERENCES

Anderson, M. P. [1984], Movement of Contaminants in Groundwater: Groundwater Transport - Advection and Dispersion, *In Groundwater Contamination, Studies in Geophysics*, National Academy Press, Washington, DC., pp. 37-45.

Belk, E. L., Markewitz, D., Radmussen, T. C., Carvaho, E. J. M., Nepstad, D. C., and Davidson, E. A. [2007], Modeling the Effects of Throughfall Reduction on Soil Water Content in a Brazilian Oxisol Under a Moist Tropical Forest, *Water Resour. Res.* Vol. 43, W08432, doi: 10.1029/2006WR005493.

Boivin, A., Simunek, J., Schiavon, M., and van Genuchten, M. Th. [2006], Comparison of Pesticide Transport Processes in Three Tile-Drained Field Soils Using HYDRUS-2D, *Vadose Zone J.*, Vol. 5, No. 3, pp. 838-849.

de Vos, J. A., Simunek, J., Raats, P. A. C., and Feddes, R. A. [1999], Identification of the Hydraulic Characteristics of a Layered Silt loam. *In* M. Th. van Genuchten, F. J. Leij, and L. Wu (eds.), *Characterization and Measurement of the Hydraulic Properties of Unsaturated Porous Media*. Univ. of California, Riverside, CA. Part 1, pp. 783-798.

Durner, W. [1994], Hydraulic Conductivity Estimation for Soils with Heterogeneous Pore Structure. *Water Resour. Res*. 30:211-223.

Focus Leaching Modelling Workgroup [1995], Leaching Models and EU Registration. Guidance Document 4952/VI/95. Commission of the European Communities, Directorate-General for Agriculture VI B II-I, Brussels, Belgium.

Gerke, H. H. [2006], Preferential Flow Descriptions for Structured Soils, *J. Plant Nutr. & Soil Sci.,* Vol. 169, pp. 382-400.

Gerke, H. H., and Köhne, J. M. [2004], Dual-Permeability Modeling of Preferential Bromide Leaching from a Tile-Drained Glacial Till Agricultural Field, *J. Hydrol*.,Vol. 289, No. 1-4, pp. 239-257.

Gerke, H. H., and van Genuchten, M. Th. [1993a], A Dual-Porosity Model for Simulating The Preferential Movement of Water and Solutes in Structured Porous Media, *Water Resour. Res*., Vol. 29, No. 2, pp. 305-319.

Gerke, H. H., and van Genuchten, M. Th. [1993b], Evaluation of a First-Order Water Transfer Term for Variably-Saturated Dual-Porosity Models, *Water Resour. Res*., Vol. 29, No. 4, pp. 1225-1238.

Hendrickx, J. M. H., and Flury, M. [2001], Uniform and Preferential Flow Mechanisms in the Vadose Zone, *In Conceptual models of Flow and Transport in the Fractured Vadose Zone*, National Academy Press, Washington, DC, pp. 149-187.

ICRP [1983], *Radionuclide Transformations: Energy and Intensity of Emissions*, Int. Commission on Radiological Protection, ICRP Publication 38, Pergamon Press, Oxford.

ISAM [1999], *Derivation of Quantitative Acceptance Criteria for Disposal of Radioactive Waste to Near Surface Facilities: Development and Implementation of an Approach,* Safety Report, Version 3.0, March 1999, IAEA, Vienna, Austria.

Jarvis, N. J. [1994], *The MACRO Model (Version 3.1), Technical Description and Sample Simulations,* Reports and Dissertations 19, Dept of Soil Science, Swedish Univ. of Agricultural Sciences, Uppsala, Sweden, 51 p.

Kodesova, R., Kozak, J., Simunek, J., and Vacek, O. [2005], Field and Numerical Study of Chlorotoluron Transport in the Soil Profile: Comparison of Single and Dual-Permeability Model, *Plant, Soil and Environ.*, Vol. 51, No. 7, pp. 310-315.

Köhne, J. M., Mohanty, B., Simunek, J., and Gerke, H. H. [2004], Numerical Evaluation of a Second-Order Water Transfer Term for Variably Saturated Dual-Permeability Models, *Water Resour. Res.*, *40*, doi:10.1029/2004WR00385.

Köhne, J. M., Köhne, S., and Simunek, J. [2006], Multi-Process Herbicide Transport in Structured Soil Columns: Experiment and Model Analysis, *J. Contam. Hydrol.* Vol. 85, pp. 1-32.

Leij, F. J., Alves, W. J., van Genuchten, M. Th., and Williams, J. R. [1996], The UNSODA Unsaturated Soil Hydraulic Database; User's Manual, Version 1.0. *EPA/600/R-96/095*, National Risk Management Laboratory, Office of Research and Development, U.S. Environmental Protection Agency, Cincinnati, OH, 103 p.

Liu, H. H., Bodvarsson, G. S., and Zhang, G. [2004], Scale Dependency of the Effective Matrix Diffusion Coefficient, Vol. 3, pp. 312-315.

Maraqa, M. A. [2001], Prediction of Mass-Transfer Coefficient for Solute Transport in Porous Media. *J. Contam. Hydrol*., Vol. 53, pp. 153-171.

Mohanty, B. P., Bowman, R. S., Hendrickx, J. M. H., and van Genuchten, M. Th. [1997], New Piecewise-Continuous Hydraulic Functions for Modeling Preferential Flow in an Intermittent Flood-Irrigated Field, *Water Resour. Res*., Vol. 33, No. 9, pp. 2049-2063.

Nemes, A., Schaap, M. G., Leij, F. J., and Wösten, J. H. M., [2001]. Description of the Unsaturated Soil Hydraulic Database UNSODA, Version 2.0. *J. Hydrol.* Vol. 251, pp. 151-162.

Nkedi-Kizza, P., Biggar, J. W., van Genuchten, M. Th., Wierenga, P. J., Selim, H. M., Davidson, J. M., and Nielsen, D. R. [1983], Modeling Tritium and Chloride-36 Transport Through an Aggregated Oxisol, *Water Resour. Res.*, Vol. 19, No. 3, pp. 691-700.

Novak, S. M., Banton, O., and Schiavon, M. [2003], Modeling Metolachlor Exports in Subsurface Drainage Water from Two Structured Soils under Maize (Eastern France), *J. Hydrol*., Vol. 270, No. 3-4, pp. 295-308.

Pachepsky, Y., Gimenez, D., Lilly, A., and Nemes, A. [2008], Promises of Hydropedology, *CAB Reviews: Perspectives in Agriculture, Veterinary Science, Nutrition and Natural Resources*, 2008 3, No. 040.

Peters, R. R., and Klavetter, E. A. [1988], A Continuum Model for Water Movement in an Unsaturated Fractured Rock Mass, *Water Resour. Res*., Vol. 24, pp. 416-430.

Pontedeiro, E. M., van Genuchten, M. Th., Cotta, R. M., and Simunek, J. [2009], The Effects of Preferential Flow and Soil Texture on Risk Assessment of a NORM Waste Disposal Site, *J. Hazadous Materials* (submitted).

Pot, V., Simunek, J., Benoit, P., Coquet, Y., Yra, A., and Martínez-Cordón, M.-J. [2005], Impact of Rainfall Intensity on the Transport of Two Herbicides in Undisturbed Grassed Filter Strip Soil Cores. *J. Contam. Hydrol.*, Vol. 81, pp. 63-88.

Schaap, M. G., Leij, F. J. and van Genuchten, M. Th. [1998], Neural Network Analysis for Hierarchical Prediction of Soil Hydraulic Properties, *Soil Sci. Soc. Am. J*.,Vol. 62, No. 4, pp.847-855.

Schaap, M. G., and van Genuchten, M. Th. [2006], A Modified van Genuchten-Mualem Formulation for Improved Prediction of the Soil Hydraulic Conductivity Function Near Saturation. *Vadose Zone J.* Vol. 5, No. 1, pp. 27-34.

Simunek, J., and van Genuchten, M. Th. [2006], Contaminant Transport in the Unsaturated zone; Theory and Modeling, *In* J.W. Delleur (ed.), *Handbook of Groundwater Engineering*, 2nd ed., CRC Press, Boca Raton, FL, pp. 22.1-46.

Simunek, J., and van Genuchten, M. Th. [2008]. Modeling Nonequilibrium Flow and Transport Processes using HYDRUS, *Vadose Zone J.*, Vol 7, pp. 782-797.

Simunek, J., Huang, K., Sejna, M., and van Genuchten, M. Th. [1999], The HYDRUS-2D Software Package for Simulating Two-Dimensional Movement of Water, Heat and Multiple Solutes in Variably-Saturated Media. Version 2.0. *IGWMC-TPS-53*, Int. Ground Water Modeling Center, Colorado School of Mines, Golden, CO., 251 p.

Simunek, J., Jarvis, N. J., van Genuchten, M. Th., and Gärdenäs, A. [2003], Review and Comparison of Models for Describing Non-Equilibrium and Preferential Flow and Transport in the Vadose Zone. *J. Hydrol*. Vol. 272, No. 1-4, pp. 14-35.

Simunek, J., van Genuchten, M. Th., and Sejna, M. [2005], The HYDRUS-1D Software Package for Simulating the One-Dimensional Movement of Water, Heat and Multiple Solutes in Variably-Saturated Media. Version 3.0. *HYDRUS Software Series 1,* Dept. of Environmental Sciences, Univ. of California, Riverside, 240 p.

Simunek, J., van Genuchten, M. Th., and Sejna, M. [2008], Development and Applications of the HYDRUS and STANMOD Software Packages and Related Codes, *Vadose Zone J.,* Vol. 7, pp. 587-600.

Truckenbrodt, W., and Kotschoubey, B. [1981], Cobertura Terciária das Bauxitas Amazônicas., *Revista Braileira Geociências,* Vol. 11, pp. 203-208.

USEPA [1996], *Soil Screening Guidance: Technical Background Document*, EPA/540/R-95/128, PB96–963502, Office of Solid Waste and Emergency Response, U.S. Environmental Protection Agency, Washington, DC.

USEPA [2004], *Drinking Water Standards and Health Advisories*, Office of Water, U.S. Environmental Protection Agency, Washington, DC, 20 p.

van Genuchten, M. Th. [1980]. A Closed-Form Equation for predicting the Hydraulic Conductivity of Unsaturated Soils*, Soil Sci. Soc. Am.*, Vol. 44, pp. 892-898.

van Genuchten, M. Th., and Dalton, F. N. [1986], Models for Simulating Salt Movement in Aggregated Field Soils, *Geoderma*, Vol. 38, pp. 165-183.

van Genuchten, M. Th., and Wagenet, R. J. [1989], Two-Site/Two-Region Models for Pesticide Transport and Degradation: Theoretical Development and Analytical Solutions. *Soil Sci. Soc. Am. J.*, Vol. 53, No. 5, pp. 1303-1310.

van Genuchten, M. Th., and Wierenga, P. J. [1976], Mass Transfer Studies in Sorbing Porous Media. I. Analytical Solutions. *Soil Sci. Soc. Am. J.*, Vol. 40, pp. 473-480.

Vogel, T., and Císlerova, M. [1988], On the Reliability of Unsaturated Hydraulic Conductivity Calculated from the Moisture Retention Curve, *Transp. Porous Media*, Vol. 3, pp. 1-15.

Vogel, T. van Genuchten, M. Th., and Cislerova, M. [2000], Effect of the Shape of the Soil Hydraulic Functions near Saturation on Variably-Saturated Flow Predictions. *Adv. Water Resour.* Vol. 24, No. 2, pp. 133-144.

Zimmerman, R. W., Chen, G., Hadgu, T., Bodvarsson, G. S. [1993], A Numerical Dual-Porosity Model with Semi-Analytical Treatment of Fracture/Matrix Flow, *Water Resour. Res*., Vol. 29, pp. 2127–2137.

Zurmühl, T., Durner, W. [1996], Modeling Transient Water and Solute Transport in a Biporous Soil, *Water Resour. Res*., Vol. 32, pp. 819–829.